

1 **The Circulation Response to Volcanic Eruptions: The Key Roles of**
2 **Stratospheric Warming and Eddy Interactions**

3 Kevin DallaSanta*, Edwin P. Gerber

4 *Center for Atmosphere-Ocean Science, Courant Institute of Mathematical Sciences,*
5 *New York University, New York, NY, USA*

6 Matthew Toohey

7 *GEOMAR Helmholtz Centre for Ocean Research Kiel, Kiel, Germany*

8 * *Corresponding author address:*

9 E-mail: dalla@cims.nyu.edu

ABSTRACT

10 Proxy data and observations suggest that large tropical volcanic eruptions in-
11 duce a poleward shift of the North Atlantic jet stream in boreal winter. There
12 is far from universal agreement in models, however, and the potential effect
13 of volcanic aerosol on the austral circulation and mechanism(s) by which they
14 impact the jets are unclear. This study examines the impact of stratospheric
15 aerosol on the circulation using a hierarchy of simplified atmospheric mod-
16 els. In particular, the models allow the separation of the dominant shortwave
17 (surface cooling) and longwave (stratospheric warming) impacts of volcanic
18 aerosol. It is found that the cooling effect of surface darkening has little im-
19 pact on the circulation, while stratospheric warming decisively shifts the jet
20 poleward in both summer and winter hemispheres.

21 Further study with simplified models demonstrates that the response to
22 stratospheric warming is remarkably generic and does not depend critically
23 on the boundary conditions (e.g., the planetary wave forcing) or the atmo-
24 spheric physics (e.g., the treatment of radiative transfer and moist processes).
25 It does, however, fundamentally involve both zonal-mean and eddy circula-
26 tion feedbacks. The timescales, seasonality, and structure of the response
27 provide further insight into the mechanism, as well as its connection to modes
28 of intrinsic natural variability. These findings have implications for the inter-
29 pretation of comprehensive model studies and for post-volcanic prediction.

30 **1. Introduction**

31 Volcanic aerosol primarily impacts Earth's climate by scattering incoming shortwave radiation
32 and absorbing and emitting longwave radiation. While aerosol in the troposphere are generally
33 washed out by the hydrological cycle within a few weeks, sufficiently large eruptions can in-
34 ject material into the stratosphere. Volcanoes emit both ash and sulfuric compounds that oxidize
35 and form H₂SO₄ aerosol droplets; it is thought that the latter is most important in the strato-
36 sphere. Following large tropical eruptions, like that of Mt. Pinatubo in 1991, the Brewer-Dobson
37 circulation lifts and meridionally spreads these droplets, allowing them to persist in the middle
38 atmosphere with an e-folding lifetime of approximately one year. The shortwave effect causes
39 globally-averaged surface cooling, while the longwave effect causes localized warming of the
40 tropical stratosphere (Robock 2000). The cooling effect of volcanoes has been appreciated for
41 centuries (e.g., Franklin 1784), but paradoxically, temperature reconstructions from proxy data
42 also indicate that much of Northern Eurasia warms during the first few winters after a large vol-
43 canic eruption, even after accounting for ENSO variability (Robock and Mao 1995; Fischer et al.
44 2007).

45 The spatial pattern of reconstructed temperature changes following past eruptions suggests a
46 positive anomaly of the Northern Annular Mode (e.g., Robock 2000). A positive annular mode
47 is characterized by a poleward shift of the extratropical jet, a stronger winter vortex, and surface
48 warming in subpolar latitudes, especially over land (Thompson and Wallace 2000). Indeed, nu-
49 merous studies with comprehensive models have reproduced a poleward jet shift in response to
50 volcanic forcing (e.g., Graf et al. 1993; Robock and Mao 1995; Barnes et al. 2016). However,
51 other studies have found a tepid or even opposite response in the NH winter (e.g., Ramachandran
52 et al. 2000; Robock et al. 2007; Driscoll et al. 2012; Marshall et al. 2009). Furthermore, fewer

53 studies have addressed the SH response, where proxy data is scarce. Some studies have found a
54 poleward shift of the SH winter jet (e.g., Karpechko et al. 2010; McGraw et al. 2016) while again
55 others have found little or opposite response (e.g., Robock et al. 2007; Roscoe and Haigh 2007).

56 In context of a large tropical eruption, a poleward jet shift has been attributed to two general
57 mechanisms: surface darkening and stratospheric warming. A first possible mechanism (Graf
58 1992; Stenchikov et al. 2002) observes that aerosol scattering of shortwave radiation dims and
59 cools the surface, reducing the tropospheric meridional temperature gradient. Assuming this re-
60 duces midlatitude baroclinicity, it is possible that upward wave flux is reduced so as to stimulate a
61 stronger vortex feeding back with a poleward shift of the jet.

62 A second possible mechanism (Robock and Mao 1995) observes that aerosol absorption of long-
63 wave radiation warms the tropical stratosphere, steepening the stratospheric meridional tempera-
64 ture gradient. At small Rossby number, this balances a westerly acceleration of the zonal winds.
65 Assuming this occurs in the midlatitudes, the vortex acceleration feeds back with a poleward shift
66 of the jet via the stratosphere-troposphere coupling reflected in the annular mode. A majority of
67 previous studies have favored this hypothesis; however, as has been noted, (Stenchikov et al. 2002;
68 Toohey et al. 2014; Bittner et al. 2016), the meridional temperature gradient may not be in direct
69 balance with a strengthened vortex. We will constructively demonstrate that the qualitative nature
70 of this hypothesis is quite sensitive to its quantitative details.

71 Given the wide variety of results obtained with comprehensive models and the inconsistent con-
72 clusions regarding mechanisms, Zanchettin et al. (2016) proposed a volcanic model intercompar-
73 ison project (VolMIP) to study this issue within the CMIP6. VolMIP details several experiments,
74 including differentiation of forcings (stratospheric warming and surface darkening) and study of
75 the steady-state and transient responses. The unified protocol will reduce methodological uncer-
76 tainty in our understanding of the response and afford the opportunity for a more complete study

77 of the atmospheric and oceanic response to volcanic forcing than has been previously undertaken.
78 However, comprehensive models have many degrees of freedom, including several sources of jet
79 variability which may mask the signal of volcanic forcing or obscure its mechanism: for instance,
80 ENSO (McGraw et al. 2016; Lehner et al. 2016), the QBO (Garfinkel et al. 2012), and ozone
81 recovery (Son et al. 2010). The latter will not be a concern for VolMIP experiments with pre-
82 scribed ozone, but all of these may come into play when comparing previous model studies with
83 one another.

84 We seek to address this challenge by examining volcanic forcing in a hierarchy of idealized
85 models, sequentially studying how each level of complexity relates to the response. The resultant
86 simplicity aids understanding of the dynamical mechanism of volcanic forcing, although as we
87 will see, causality is not always clear in the nonlinear atmosphere.

88 We first investigate the equilibrium responses to the two aerosol impacts in a moist aquaplanet
89 model with fairly realistic zonal asymmetries in the surface conditions. We find that the observed
90 circulation response is driven by tropical stratospheric warming, not surface cooling. Next, we
91 simplify our model in order to understand the mechanistic roles played by planetary-scale waves,
92 radiative transfer and moist physics, synoptic eddy feedbacks, and the zonal-mean circulation.
93 Additional insight into the mechanism is provided by the temporal evolution in response to instan-
94 taneous forcing. Finally, we will relate the forced response of these models to their internal modes
95 of variability.

96 **2. The circulation response to surface darkening versus stratospheric warming**

97 We start with the equilibrium response to surface darkening and stratospheric warming in a
98 recently developed aquaplanet general circulation model. MiMA (a Model of an idealized Moist
99 Atmosphere, Jucker and Gerber 2017) is an extension of GRAM (Gray Radiation Aquaplanet

100 Moist general circulation model, Frierson et al. 2006). Briefly, MiMA includes the simplified
101 hydrological cycle of GRAM, but replaces the single-stream “gray” radiative transfer scheme with
102 a full radiation package, RRTM (Rapid Radiative Transfer Module, Mlawer et al. 1997; Iacono
103 et al. 2000). The chief simplification of MiMA relative to comprehensive models is to neglect
104 the effect of clouds: any condensed moisture (convective and resolved) falls out immediately,
105 eliminating the role of microphysics in the hydrological cycle and radiative transfer. Consequently,
106 MiMA is among the simplest models able to simulate both shortwave and longwave perturbations.
107 As configured, its radiatively active gases are water vapor (a prognostic variable), carbon dioxide
108 fixed at 300 ppm, and stratospheric ozone fixed at 1990-averaged values.

109 We begin with a fairly realistic configuration of the model. The lower boundary includes ob-
110 served topography and land-sea contrast is approximated by variations in the heat capacity of the
111 “slab ocean” surface mixed layer. The mixed layer includes a fixed meridional heat flux in the trop-
112 ics to approximate ocean heat transport there; thus by construction there is no ENSO. The diurnal
113 and annual variations in insolation are forced and the Alexander and Dunkerton (1999) gravity
114 wave parameterization is included, which helps spontaneously generate a QBO-like oscillation
115 of periodicity roughly 36 months. To illustrate the impact of these variations on the circulation,
116 Figure 1 shows the storm tracks of the model. While the asymmetry between the North Atlantic
117 and North Pacific storm tracks is not fully realized, this configuration of MiMA does capture the
118 dominant stationary wave patterns and localization of the storm activity in both hemispheres, in
119 addition to their variation within the annual cycle.

120 Our setup is designed to mimic the surface darkening and stratospheric warming that occurred
121 after the eruption of Mt. Pinatubo in 1991. We apply these forcings separately to focus on the dy-
122 namics of each. Additional testing found that the response to both simultaneously is approximately
123 the superposition of the individual responses.

124 For surface darkening experiments, we reduce the solar constant by 0.5 %, producing a global
 125 mean net radiative forcing of approximately -1.7 W m^{-2} , comparable to the mean net radiative
 126 forcing averaged over the eruption of Mt. Pinatubo, which peaked at about 3 W m^{-2} (Minnis et al.
 127 1993). This prescribed forcing also produces surface cooling similar to the observed peak global
 128 surface cooling of 4 K (Thompson et al. 2009). A more realistic setup in which the darkening
 129 varied for each latitude is not possible in MiMA’s current configuration.

130 For stratospheric warming experiments, we directly apply a zonal-mean temperature tendency
 131 identically for each timestep to the lower stratosphere. This is an idealized approximation to
 132 simulations of the Mt. Pinatubo eruption period (Toohey et al. 2014) using prescribed aerosol
 133 properties from the SAGE_4 λ reconstruction. Explicitly, the tendency is

$$\sum_i a_i \exp\left(-\frac{(\phi - \tilde{\phi}_i)^2}{2\sigma_i^2} - \frac{(z - \tilde{z}_i)^2}{2\zeta_i^2}\right) \quad (1)$$

134 with parameter values given in Table 1.

135 Recent work indicates that the heating profiles produced by models using the SAGE_4 λ forcing
 136 data may be somewhat overestimated (Revell et al. 2017). In any case, we find in testing that our
 137 results are linear at this magnitude of forcing, when a jet shift is triggered. Additionally, in further
 138 testing our results seem to be robust to the parameter values and number of overlaying Gaussians
 139 constituting the idealized approximation.

140 We focus first on the equilibrium DJF responses to steady forcing based on 100-year runs and
 141 return later to the responses’ temporal evolution and interseasonal structure. For these runs, MiMA
 142 is implemented spectrally at T42 truncation with 40 vertical levels up to 0.01 hPa. Runs tested with
 143 higher vertical and horizontal resolutions yield very similar results.

144 Figure 2 shows the temperature and zonal responses in MiMA to surface darkening and strato-
 145 spheric warming. For darkening (Figure 2a,c), the entire troposphere cools significantly, with

146 globally-averaged surface temperatures reduced by 0.9 K. This magnitude is greater than the
147 ENSO-adjusted response to the eruption of Mt. Pinatubo (Thompson et al. 2009), but is within
148 the linear regime of our model response, based on additional testing. The stratospheric temper-
149 ature response is weak, except for cooling in the upper stratosphere over the winter pole, which
150 indicates additional downwelling there.

151 In the zonal wind field (Figure 2b,d), the only significant response is a slight deceleration of both
152 subtropical jets, as would be expected with a lowering of the tropopause in response to tropospheric
153 cooling. If anything, the SH jet tends to shift equatorward in austral winter, opposite (and therefore
154 consistent with) the projected poleward shift associated with global warming (Yin 2005). Given
155 the large sample size (100 winters), the lack of a clear jet shift leads us to conclude that surface
156 darkening has little effect on lower tropospheric winds.

157 MiMA's response to surface darkening contrasts the response found by Stenchikov et al. (2002).
158 They simulated a latitudinally-dependent tropospheric cooling in a comprehensive general circu-
159 lation model also with realistic zonal asymmetries, but with only 4 ensemble members. Their
160 surface darkening reduced mid-latitude Eliassen-Palm flux by one standard deviation, stimulating
161 a stronger vortex and poleward jet shift in the winter hemisphere. Given that the effect is not
162 reproduced in our simpler model and a paucity of other studies have addressed darkening, care is
163 necessary when performing intermodel comparisons such as VolMIP aims to do.

164 In contrast to surface darkening, stratospheric warming (Figure 2f,h) accelerates the strato-
165 spheric vortex and shifts the tropospheric jet polewards in both winter hemispheres. This is consis-
166 tent with the statistically significant poleward shift of the winter jet inferred from proxy data. In the
167 stratosphere, the winter vortex strengthens, while the quiescent summer stratosphere also exhibits
168 a westerly anomaly. In the troposphere, the jets move poleward in both winter hemispheres, with
169 some separation of the subtropical and eddy-driven components. The SH jet also shifts poleward

170 during summer, but the weaker NH summer jet remains roughly the same. As we will discuss,
171 the wind response projects strongly onto existing modes of variability in the troposphere and in
172 some cases the stratosphere. Lastly, we remark that the model’s QBO-like oscillation shuts down
173 in response to the prescribed stratospheric warming. This is not unheard of for models (Niemeier
174 and Schmidt 2017), but should not necessarily be interpreted as the expected response in the real
175 world.

176 The temperature response (Figure 2e,g) is consistent with other modeling studies (e.g., Toohey
177 et al. 2014; Revell et al. 2017). It shows the direct warming applied in the tropical stratosphere
178 as well as indirect heating of the high winter stratosphere over the poles, indicating an overall
179 weakening of the meridional circulation there, as in Toohey et al. (2014). Equatorial changes
180 above 20 hPa are associated with the QBO shutdown and are not essential to the mechanism, as
181 we will see for a simplified configuration of MiMA.

182 To summarize, MiMA responds to stratospheric warming with a strengthened vortex and a pole-
183 ward shift of the winter and SH summer jets, while the darkening response is a tepid weakening
184 of the subtropical jets, as might be anticipated from global cooling. While there may be other
185 processes in the atmosphere that could induce a poleward shift of the jet in response to darken-
186 ing, stratospheric warming appears qualitatively—moreover quantitatively—sufficient to capture
187 the jet shift. Hence, for the remainder of this study we focus on the warming experiments and
188 examine the mechanism behind these anomalies with a hierarchy of simpler models.

189 **3. Insufficiency of the “thermal wind balance” hypothesis**

190 Previous discussions of the mechanism (e.g., Robock and Mao 1995; Stenchikov et al. 2002)
191 focus on the meridional temperature gradient in the lower stratosphere. We state the hypothesis
192 as follows: aerosol warming of the tropical stratosphere steepens the equator-to-pole temperature

193 gradient. As the stratosphere remains balanced, this is associated with an acceleration of the
 194 wintertime vortex. To impact the troposphere, eddy feedbacks connect the vortex acceleration
 195 with a poleward shift of the tropospheric jet, as with the response to SH ozone loss (Son et al.
 196 2010) or natural variability (Baldwin and Dunkerton 2001).

197 A key assumption of this hypothesis is that the stratospheric temperature response balances an
 198 acceleration of the winter vortex. Although the temperature and zonal wind fields in the extratrop-
 199 ical stratosphere are well-balanced a posteriori as a consequence of small Rossby number NH/f ,
 200 there is no a priori guarantee that the warming response will accelerate the vortex region. The
 201 stratosphere may also actively respond with zonal-mean circulation adjustments. Additionally,
 202 the hypothesis focuses on the effect in the winter hemisphere without addressing whether similar
 203 reasoning might apply in the summer stratosphere where the winds are quiescent.

204 To explore the limitations of this mechanism, we start with a “straw man” argument, examining
 205 the impact of aerosol-induced stratospheric warming in the limit of fixed dynamical heating. To
 206 first order in Rossby number, the atmosphere is in thermal wind balance and the zonal-mean
 207 response is given by

$$\Delta u(\phi, p) = -\frac{1}{f(\phi)} \int_{\text{surface}}^p \frac{R}{ap'} \frac{\partial}{\partial \phi} \Delta T(\phi, p') dp' \quad (2)$$

208 where Δ indicates perturbation minus control. The key to making a prediction with this mechanism
 209 is to obtain an a priori prediction of ΔT .

210 As shown in the following section, the circulation response can be recovered in a simple Held
 211 and Suarez (1994) type model where radiation is replaced by Newtonian relaxation towards an
 212 equilibrium temperature T_{eq} as $\frac{\partial T}{\partial t} = \dots - \tau^{-1}(T - T_{\text{eq}})$, where $\tau(\phi, p)$ is a “radiative relaxation”
 213 timescale. Assuming there are no circulation feedbacks, the temperature response $\Delta T(\phi, p)$ in
 214 this simple context is just $F(\phi, p)\tau(\phi, p)$, where F is our prescribed warming. We scale F to

215 obtain the same amplitude temperature response as in MiMA, although this change is immaterial
216 since the balanced response is linear. We use the semi-empirical τ of Jucker et al. (2014), which
217 was optimized to provide an ideal approximation to real radiative transfer, although the uniform
218 stratospheric $\tau = 40$ days to which the Held and Suarez (1994) model defaults gives qualitatively
219 similar results. To compute Δu , we assume no change in surface winds and integrate vertically to
220 the top of the atmosphere.

221 Figure 3a,b shows the response in temperature and wind, respectively. We see that the temper-
222 ature anomaly qualitatively resembles the results obtained in the previous section (Figure 2e,g),
223 but its gradient balances a strong acceleration of merely the stratospheric winds equatorward 45°
224 rather than of the desired polar vortex acceleration. As Bittner et al. (2016) emphasized, the strato-
225 spheric response evidently involves eddy feedbacks. To investigate them, we examine a series of
226 simplifications bridging the gap between MiMA and fixed dynamical heating.

227 **4. The processes linking stratospheric warming to tropospheric jet shifts**

228 The response to stratospheric warming alone in our aquaplanet model MiMA broadly agrees
229 with observations and many comprehensive model studies. In the stratosphere, the polar vortex
230 is enhanced well beyond a naïve thermal wind response, and in the troposphere, the winter and
231 summer jets expand poleward. To identify the relevant processes driving these effects, we apply
232 three successive simplifications to the model.

233 *a. Zonally symmetric lower boundary*

234 Do planetary waves play an essential role in the response? Some previous studies (e.g., Perl-
235 witz and Graf 1995) have suggested an affirmative answer, pointing to their role in stratosphere-
236 troposphere coupling. To address this, we first replace the realistic topography and land-sea con-

237 trast with a uniform lower boundary condition, and replace the gravity wave parameterization
238 with a simple Rayleigh damping layer near the model top. (The gravity wave scheme was omitted
239 largely because it must be re-tuned considerably when planetary waves are omitted, but as will
240 be found, this change suggests that the details of the gravity wave driving are not essential to the
241 response.) The model still spontaneously generates planetary waves, as energy scatters up from
242 baroclinic instability, but the overall planetary wave activity is greatly diminished. As a result, the
243 stratospheric polar vortices become very strong and steady in the winter hemisphere; in particular,
244 sudden stratospheric warmings in the zonally asymmetric configuration are no longer observed.

245 Figure 3c,d shows the temperature and zonal wind responses in this configuration. Both are
246 qualitatively similar to the zonally asymmetric configuration (Figure 2e–h); note that with this
247 hemispherically symmetric version of the model, austral winter is simply a reflection of boreal
248 winter. Quantitatively, the response is stronger with the reduction of wave forcing, in agreement
249 with the findings of Toohey et al. (2014) that wave forcing acts as a negative feedback to the heating
250 anomalies. In the zonal wind field, the response also aligns well with the model’s existing modes
251 of variability in the troposphere and winter stratosphere: a poleward jet shift in both hemispheres
252 and a strengthened winter stratospheric vortex. This configuration of the model does not produce a
253 QBO-like oscillation, primarily due to the lack of realistic gravity wave driving, so the response of
254 the tropical winds is vaguely reminiscent of a “frozen” QBO. We conclude that neither the details
255 of the climatology nor topographically-forced stratospheric-tropospheric coupling is essential for
256 the circulation response to stratospheric warming.

257 *b. Simplified physics and no annual cycle*

258 If the details of the planetary waves (or gravity wave drag) are not necessary, what about moist
259 and radiative processes? To investigate, we turn to the Held and Suarez (1994) dry dynamical core.

260 It shares the same primitive equation dynamics, psuedo-spectral numerical implementation, flat
261 lower boundary, and Rayleigh damping at the model top as the previous configuration of MiMA.
262 All diabatic physics, however, are replaced by Newtonian relaxation of the temperature field to an
263 equilibrium DJF profile specified by Polvani and Kushner (2002), and discussed previously in the
264 context of the fixed dynamical heating argument.

265 Applying stratospheric warming to this highly idealized atmospheric model, we see qualita-
266 tively the same response as in MiMA (Figure 3e,f). The temperature response in the stratosphere
267 is slightly narrower, which corresponds with an equatorward movement of the stratospheric wind
268 anomalies, but in the troposphere, we see the characteristic poleward shift of the tropospheric jets,
269 although the magnitude is smaller. This demonstrates that the details of radiative and moist pro-
270 cesses are not essential to the circulation response to stratospheric warming, but suggests that di-
271 abatic effects could amplify the response. As in MiMA, the circulation response projects strongly
272 onto the model's existing modes of variability; this can explain the quantitative differences in the
273 troposphere and will be discussed in Section 6. Lastly, we note that like the zonally symmetric
274 configuration of MiMA, this model does not have a QBO-like oscillation, and it has a comparable
275 response of the tropical stratosphere.

276 *c. The role of eddies*

277 Given that highly simplified physics (but not thermal wind balance) suffices to produce a vor-
278 tex acceleration and a poleward jet shift, what circulation feedbacks are involved? Specifically,
279 is the circulation response fundamentally three-dimensional (i.e., involving eddies), or could an
280 axisymmetric theory suffice, as for example with the Hadley cell theory of Held and Hou (1980)?
281 We address this by axisymmetrizing the previous configuration of the dry dynamical core. We
282 follow the procedure of Kushner and Polvani (2004), which allows us to apply the heating about a

283 configuration with the same zonal-mean circulation as the full three-dimensional model. Briefly,
284 one initializes the three-dimensional model with the desired zonal-mean state, and then runs it for
285 one time step to compute the zonally-asymmetric tendency of the model to leave this state. Then
286 this tendency is subtracted at each and every timestep; the result is a steady model (excepting a
287 few small high frequency vibrations) that shares a nearly identical climatological zonal-mean with
288 the three-dimensional configuration. However, any forcing response (in our case, to stratospheric
289 warming) will only affect the zonal-mean circulation: by construction there is no eddy response.

290 The response to stratospheric warming (Figure 3g,h) in this model exhibits a decidedly more
291 narrow temperature anomaly compared to the full three-dimensional model. A Hadley cell-like
292 axisymmetric circulation does extend the warming poleward beyond that found in the limit of
293 fixed dynamical heating (compare to Figure 3a), leading to a profound change in the zonal wind
294 field (compare to Figure 3b), but does not project well onto the vortex in comparison to the three-
295 dimensional model (Figure 3f). Evidently eddy feedbacks act to meridionally widen the temper-
296 ature response, and the slight alteration of the temperature response caused by inhibiting eddy
297 feedbacks induces a large qualitative change in the zonal wind response. Furthermore, the trop-
298 ics do not respond with a QBO-like anomaly as they do for the three-dimensional models, as the
299 relevant eddy feedbacks are suppressed.

300 The axisymmetric response in the troposphere is extremely small; in particular the lower tropo-
301 sphere has no significant response. Hence eddy feedbacks are necessary to couple the stratospheric
302 response to the troposphere, but also to achieve the stratospheric response alone, supporting the
303 conclusions of Bittner et al. (2016). We examine the timescales of this coupling, and its relation
304 to internal modes of variability, in the subsequent sections.

305 *d. Interpretation*

306 Considering these results hierarchically, we find that the details of the stationary waves or strato-
307 spheric variability are not essential to capturing the response to warming, nor are the details of
308 moist and radiative processes. These factors clearly influence the quantitative structure of the
309 response, and we will return to these differences in Section 6, where we find that much can be
310 explained by differences in the natural variability across the integrations. Eddies, however, are
311 essential not only for coupling the stratospheric response to the troposphere, but for obtaining the
312 stratospheric response as well.

313 To better quantify the impact of eddy feedbacks, we plot in Figure 4 the response of the merid-
314 ional circulation in the full and axisymmetrized configurations of the dynamical core. In the
315 three-dimensional case, this is the difference Δ in residual streamfunction ψ^* . In the axisymmetric
316 configuration, the eddy term in the residual streamfunction is fixed, so $\Delta\psi^* = \Delta\psi$ where ψ is the
317 Eulerian streamfunction.

318 In the tropical stratosphere of both models, the overturning circulation increases, acting to
319 broaden the temperature anomaly in the meridional plane (similar to a Hadley cell), but eddy
320 feedbacks enhance the poleward extension of the anomaly. The anomalous overturning is much
321 more confined in the axisymmetric configuration, where the circulation can bend angular momen-
322 tum surfaces in the tropics and subtropics to redistribute the warming. As the eddy forcing is fixed
323 in this model, the circulation cannot cross angular momentum surfaces into the extratropics.

324 The stratospheric response in the three-dimensional model is more complicated above and pole-
325 ward of the heating region due to changes in wave breaking around the NH winter vortex. In
326 particular, the overturning circulation over the pole weakens, consistent with an equatorward shift
327 in wave driving that helps increase the circulation in the tropics.

328 Recalling that the troposphere responds little in the axisymmetric configuration because of the
329 fixed eddies, the tropospheric responses are informative but should not be directly compared. The
330 response in the three-dimensional model bears the signature of the jet shift: the overturning weak-
331 ens in the tropics, but positive anomalies show up in the extratropics, associated with a poleward
332 shift of the jet and Ferrel cell.

333 We have tried different widths of the stratospheric heating profile and found qualitatively sim-
334 ilar results, but there does not appear to be a simple relation between the shape of the heating
335 and the shape or strength of the circulation response. For example, a straightforward application
336 of the Held and Hou (1980) theory is not possible, even in the zonally symmetric model. The
337 tropospheric response does, however, scale fairly linearly with the strength of the warming. Fig-
338 ure 5 highlights the linearity of the tropospheric response in the zonally symmetric configuration
339 of MiMA, and shows that our control warming amplitude falls within the linear regime of the
340 forcing. In fact, the response saturates only slightly when the forcing is doubled, more so in the
341 winter hemisphere than the summer hemisphere, even though the response is already significantly
342 smaller in the winter hemisphere.

343 **5. Timescale of the circulation response to stratospheric warming**

344 The previous section establishes that the stratospheric response to warming can be captured with
345 highly simplified physics, but that it does require eddy feedbacks. Given that volcanic forcing (at
346 least as prescribed in atmospheric models) evolves on timescales of months to years, while eddies
347 turn over on a timescales of 3–5 days (even in the stratosphere), causality in the atmosphere is
348 difficult to assess. One approach is to examine the adjustment time for different regions of the
349 atmosphere after an eruption. We investigate this temporal evolution of the warming response by
350 running a series of switch-on experiments. For both MiMA (using the original configuration with

351 topography) and the dynamical core, we create a 100-member ensemble of 2-year runs branching
352 off from the control run with an abrupt application of warming that is then held constant. This
353 is somewhat analogous to a real eruption, but we are simplifying the temporal development by
354 treating aerosol forcing as a Heaviside function. For the MiMA ensemble, which has an annual
355 cycle, forcing is applied beginning on January 1; limited testing with other start dates leads to very
356 similar results.

357 *a. The fast extratropical response*

358 Figure 6 shows the evolution of the zonal wind responses in two models at 35 hPa, through
359 the core of the warming, and 850 hPa, an ideal level to track the extratropical eddy-driven jets.
360 In MiMA (the configuration with the more realistic lower boundary conditions is shown), we
361 see a relatively quick convergence of the extratropical stratosphere to the equilibrium, seasonally
362 evolving response, with a lag of at most 2–3 months. The associated signal in the troposphere lags
363 that of the stratosphere (very slightly in the NH but much more in the SH), however quantifying the
364 lag is complicated by the presence of the annual cycle. It does appear well-converged within one
365 year. These results imply that the extratropical atmosphere reaches the equilibrium state within
366 the lifetime of the aerosol forcing (1–3 years), although slow ocean feedbacks may play a role on
367 longer timescales in the real atmosphere.

368 The dynamical core simulations are easier to interpret, as there is no seasonal cycle. The lag of
369 the tropospheric winds behind the extratropical stratospheric winds is readily apparent, particularly
370 in the winter (Northern) hemisphere. The simplified boundary conditions (and hence less internal
371 variability, particularly in the stratosphere) may also play a role in amplifying the tropospheric
372 lag; results in the MiMA configuration without topography (not shown) appear to show a greater
373 tropospheric lag in comparison with the zonally asymmetric configuration. We speculate that

374 stationary waves tighten the dynamical coupling between the troposphere and stratosphere. They
375 also impact the tropospheric variability directly, however, which could affect their sensitivity and
376 response time.

377 To quantify these results more precisely in the dynamical core integrations, we project the zonal
378 wind response as a function of time onto the equilibrium response (Figure 7). Interpretation of
379 the adjustment time is simpler for the dynamical core since it runs in perpetual winter; applying
380 the same metric in MiMA suffers from a lower signal-to-noise ratio and the complication of the
381 annual cycle. We see that the stratosphere immediately begins adjustment towards equilibrium
382 on a timescale of 1–2 months, but the tropospheric jets have little response for approximately
383 2 weeks and then converge on a slower timescale of 4–10 months. In both the stratosphere and the
384 troposphere, the winter response is evidently slower than the summer response by roughly a factor
385 of 2, despite winter and summer responses having similar magnitude. This is qualitatively opposite
386 to the response in MiMA, emphasizing the role of stationary waves in setting the adjustment
387 timescale.

388 We conclude that warming of the tropical stratosphere drives a rapid response in the extratropical
389 stratosphere, while the tropospheric response converges on a longer timescale. This is consistent
390 with a top-down mechanism, where the polar vortex modifies the eddy-driven jet as found with
391 the annular mode response to sudden stratospheric warmings (e.g., Baldwin and Dunkerton 2001)
392 and the response to ozone loss and recovery (e.g., Polvani et al. 2011). The large response of
393 the stratospheric vortex at height, however, may be a red herring. Rather, the similar response
394 of the summer jets suggests that it is the more subtle change in winds in the lower stratosphere
395 that matter. This is the region of the stratosphere in direct contact with synoptic variability. The
396 lifecycle experiments of Wittman et al. (2004) show that tropospheric wave breaking (which in turn
397 controls the momentum fluxes) is sensitive to winds in the upper troposphere/lower stratosphere

398 region. This points to a mechanism that can operate in all seasons, and indeed, the response to
399 ozone loss and recovery in the SH peaks in late spring to summer.

400 *b. The slow tropical response*

401 Figure 7 hints at a possible “over-response” of the tropospheric circulation in the second year,
402 where the overall projection exceeds the final climatological response. All curves will eventu-
403 ally asymptote to 1 by construction. Even with 100 ensemble members, however, there is still
404 considerable internal variability, so we investigate this more closely. Figure 8b indicates that the
405 second-year response in the winter hemisphere is larger than the equilibrium response, albeit with
406 only marginal statistical confidence.

407 While the extratropical response of the circulation is largely on the timescale of weeks to
408 months, Figure 7 shows that the tropical stratosphere in the dynamical core requires a much longer
409 timescale to adjust. The winds here ultimately require about a decade to fully converge. The slow
410 evolution from tropical stratospheric easterlies to westerlies, shown in Figure 8a and c, is associ-
411 ated with the adjustment time of the balanced response, which scales inversely with the Coriolis
412 parameter (Holton et al. 1995). A decade is quite extreme—as noted below in the context of
413 MiMA, the presence of an annual cycle limits the slow adjustment—but this is the region of the
414 atmosphere that supports the QBO, which evolves on timescales orders of magnitude longer than
415 the extratropical stratosphere.

416 Although the second year and steady-state responses at the equator are small and nearly equal
417 at 35 hPa, they are large and of opposite sign at 10 hPa (Figure 8a,c). The QBO-like difference in
418 the stratosphere and small difference in the jet is in rough quantitative agreement with the find-
419 ing of Garfinkel et al. (2012), who suggest that the QBO modifies the surface winds through the
420 meridional circulation in the subtropics. In support of this mechanism, the extratropical strato-

421 spheric vortex is fairly well-converged after one year, suggesting that it is not simply a Holton
422 and Tan (1980)-type impact through the extratropical stratospheric vortex. Rather, the long-term
423 evolution of the tropical stratosphere is associated with a slight decrease of the initial extratropical
424 tropospheric response.

425 The tropical stratosphere also adjusts slowly in the configuration of MiMA without topography
426 (not shown), although the addition of the annual cycle accelerates the process to some degree. The
427 topographic configuration exhibits a faster tropical adjustment of a few years (Figure 6), consistent
428 with the timescale of the QBO. It is possible that volcanic eruptions may alter the QBO by mod-
429 ifying the dynamics of tropical wave activity, which can in turn impact the surface. This would
430 still be possible within the 1–3 year lifetime of stratospheric aerosol, and further investigation may
431 be possible with proposed model intercomparison projects with comprehensive models that can
432 capture the QBO in a forced warming state.

433 *c. Seasonality of the response*

434 The lag in the tropospheric response, 1–3 months, is sufficiently long that the circulation may not
435 reach an equilibrium at any point in the annual cycle. We consider in Figure 9 the seasonality of the
436 response using MiMA, which shows the composited transient response of zonal wind for the first
437 twelve months after a January 1 “eruption” (i.e., an abrupt initiation of heating rate anomalies) in
438 the flat configuration. Interpretation is easier with this configuration of the model; as the response
439 has essentially converged by the second half of the year, we can use June–December to observe
440 the full response over a solstitial and equinoctial season, since the lower boundary is flat in both
441 hemispheres.

442 The first few months show the initial response of the stratosphere; while a small tropospheric
443 signal is present during this time, the contour intervals were chosen to emphasize magnitudes

444 larger than than 1 ms^{-2} . The stratospheric response is initially more hemispherically symmetric
445 (January), while in just a few months (March), the presence of the winter vortex leads to amplified
446 anomalies at height in the winter (boreal) hemisphere. The response at 100 hPa—which is most
447 critical for stratosphere-troposphere coupling—is remarkably similar in both hemispheres at all
448 times of the year, and so appears to be connected with the essential response to warming in the
449 lower stratosphere.

450 The response of the winds at height, which tend to dominate the picture, are largely dictated by
451 the annual cycle of the vortices, which act as valves to planetary wave propagation into the mid
452 and upper stratosphere. At all times, the winds accelerate on the equatorward flank of the vortex,
453 peaking in amplitude at the very end of its lifecycle in late spring, as it shrinks towards the pole
454 before vanishing. (Note that vortex is long-lived in this configuration, given the lack of planetary
455 wave forcing.) This structure is associated with a concomitant equatorward shift in the wave
456 breaking and critical lines, which form along the edge of the vortex. While it is tempting to fall
457 back on the thermal wind argument (where tropical warming increases the temperature gradient,
458 accelerating the winds and bending waves equatorward), we stress that it is only valid a posteriori,
459 requiring the nonlinear dynamics of the the three-dimensional models. The end result is consistent
460 with wave refraction and wave driving arguments, but not easy to predict a priori.

461 The tropospheric response tends to maximize in solstitial seasons, weakening most notably in
462 spring. For the solstitial seasons, the 1–3 month lag is sufficiently short for the circulation to fully
463 spin up before the annual cycle changes the basic state. As seen in Figure 2f and h, we note that the
464 situation is more complicated in the more realistic configuration of MiMA, and a boreal summer
465 tropospheric response is notably absent, consistent with findings from comprehensive models (e.g.,
466 Barnes et al. 2016). The stratospheric evolution is similar in the more realistic configuration
467 model, although the enhanced planetary wave activity shortens the lifetime of the polar vortices in

468 the spring, further localizing the middle and upper stratospheric wind anomalies to the solstitial
469 seasons (not shown). The shutdown of the QBO-like oscillation in this configuration admittedly
470 complicates the analysis (essentially, reducing our effective sample size), but the early evolution
471 of the extratropical response appears to be insensitive to the initial phase of the QBO.

472 **6. Linking the response to volcanic forcing with the internal variability of the atmosphere**

473 A number of studies have highlighted connections between the response to volcanic eruptions
474 and the annular modes of variability (e.g., Perlwitz and Graf 1995; Bittner et al. 2016; Barnes et al.
475 2016; McGraw et al. 2016). The annular modes dominate variability in the extratropical atmo-
476 sphere in both hemispheres (Thompson and Wallace 2000), and have been linked to the response to
477 external forcings, including greenhouse gases (e.g., Kushner et al. 2001) and stratospheric ozone
478 (e.g., Son et al. 2010). Ring and Plumb (2007) highlight the fact that the atmosphere often re-
479 sponds modally to external forcings, and Garfinkel et al. (2013) suggest that the annular modes
480 can be used to quantify the strength and structure of eddy-vortex-jet interactions, which we have
481 shown to be critical in understanding the circulation response to stratospheric warming.

482 As we have focused thus far on the response of the polar vortices and tropospheric jets, we
483 focus on the relation to natural variability by constructing the annular modes from the zonal wind
484 fields. A similar picture emerges if we use geopotential height, which is more commonly used to
485 characterize the annular modes. We define the annular mode index on each individual pressure
486 level to be the leading principal component of 10-day lowpass-filtered daily zonal-mean zonal
487 wind anomalies poleward of 30° , latitude-weighted to account for sphericity. These anomalies are
488 taken with respect to the control climatology, which evolves seasonally in the MiMA runs. The
489 index is defined separately for the JJA and DJF seasons, allowing us to compare directly with pre-
490 existing variability in that season. After normalizing the annular mode index to have unit variance,

491 we obtain the annular mode patterns by regressing the original (unweighted) zonal-mean zonal
492 winds onto the index. With this convention, the annular mode pattern has physical units of m s^{-1}
493 and amplitude corresponding to one standard deviation σ of variability.

494 We compare the structure and amplitude of the circulation response to stratospheric warming in
495 both MiMA and the dynamical core in Table 2. For the runs without topography, by symmetry
496 we need only consider one solstice season (DJF). We report one stratospheric level: 35 hPa, which
497 captures the variability and response of the polar vortex, and one tropospheric level: 850 hPa,
498 which best captures the variability and response of the eddy driven flow of the troposphere. The
499 results are qualitatively similar for other levels within the stratosphere/troposphere, respectively.
500 The Variance columns of Table 2 tabulate the fraction of variance captured by the annular mode
501 the control run. We see that the annular mode dominates the natural variability of the zonal-mean
502 zonal wind in all seasons at both levels. We now examine the pattern correlation ρ between these
503 modes and the warming responses in the forced experiments, as well as the response amplitude A
504 in units of one standard deviation of natural variability.

505 The first two rows of Table 2 compare the circulation response to stratospheric warming with
506 the natural variability in boreal winter in our more realistic configuration of MiMA. In the NH, the
507 response nearly perfectly aligns with the annular mode structure, with a pattern correlation close
508 to unity at both 35 hPa and 850 hPa. Relative to the natural variability, however the NH response
509 is comparatively weak: equivalent to 0.47σ in the stratosphere, and even smaller ($A_{850} = 0.23\sigma$)
510 in the troposphere. This weak signal is consistent with the difficulty of isolating the response in
511 comprehensive models.

512 Under a difference of means test, the number of independent samples required to reject the null
513 hypothesis at 95 % for a signal of this strength is 81. The annular mode in the lower troposphere
514 tends to decay on a time scale of order 10–15 days, so one could expect 6–10 effective samples per

515 season, hence requiring on the order of 10 volcanic and non-volcanic winters to unambiguously
516 detect the signal. This is well within the sample size of our study, but larger than that afforded by
517 most comprehensive model studies. In the observational record, the climatology of non-volcanic
518 winters is well-sampled, so the required sample size of post-eruption winters to detect a signal
519 of this magnitude is halved. Note, however, that our forcing is strong relative to observations of
520 Pinatubo, so that 5 samples may be an optimistic estimate.

521 In the SH, the tropospheric response also aligns almost perfectly with the natural variability
522 ($\rho_{850} = 0.99$), and compared to natural variability is three times as strong as in the NH. In the
523 stratosphere, however, the response does not overlap very well with the structure of natural vari-
524 ability. In the austral winter, the SH response is remarkably similar: near-perfect alignment in
525 the troposphere (albeit weaker relative to natural variability), with a poorer overlap in the strato-
526 sphere. In the NH, the tropospheric response is decidedly different from the annular mode, as seen
527 in Figure 2f.

528 The more idealized models are remarkably consistent with the results of the comprehensive
529 model: (i) the tropospheric response generally aligns very well with the annular mode variability,
530 more so than the stratospheric response; (ii) the response is weaker relative to the amplitude of
531 natural variability in the troposphere than the stratosphere; and (iii) the winter response is generally
532 smaller relative to natural variability than the summer response. We interpret these observations
533 as follows:

- 534 i. The stratospheric response is influenced by the structure of the warming perturbation and
535 residual circulation response thereto (Toohey et al. 2014)—and so deviates from the structure
536 of natural variability—while the tropospheric response (at least in our models) is exclusively
537 driven by the eddy coupling characterized by the annular mode.

538 ii. The relative strength of the response in the stratosphere is also consistent with the fact that
539 the residual circulation there is directly forced. The weaker tropospheric response matches
540 the reduced amplitude of the tropospheric response to natural variability, such as sudden
541 stratospheric warmings (e.g., Baldwin and Dunkerton 2001).

542 iii. The relative increase of the signal-to-noise ratio of the response in summer compared to win-
543 ter is consistent with the relative lack of variability in the summer hemisphere. The stronger
544 amplitude (in an absolute sense, see Figure 2f,h) also lines up with the enhanced temporal
545 variability of the annular mode (Garfinkel et al. 2013).

546 By calling the consistency across models “remarkable,” we emphasize that the variability (and
547 response) change dramatically across these integrations. The degree of consistency suggests a
548 generic relationship between the response and variability. To illustrate this point, Figure 10 shows
549 two examples comparing a two-dimensional annular mode with the circulation response. Here, the
550 annular mode overlays the NH DJF warming response in MiMA for both configurations previously
551 described.

552 As shown by Gerber and Polvani (2009) Figure 7, the annular mode structure changes dra-
553 matically with the lower boundary conditions, shifting from a troposphere-dominated mode (Fig-
554 ure 10b) to stratosphere-troposphere coupled mode (Figure 10a) with the addition of planetary
555 wave forcings. This mirrors the difference between the observed Northern and Southern annu-
556 lar modes (e.g., Thompson and Wallace 2000, Figure 1). The response to warming (Figure 10)
557 shares this qualitative difference, extending more strongly into the troposphere in the flat configu-
558 ration than in the configuration with topography. It also shifts in latitude, corresponding with the
559 latitudinal shift in natural variability between the integrations.

560 **7. Conclusions**

561 We have investigated the shortwave and longwave effects of idealized forcings associated with
562 volcanic aerosol on the atmospheric circulation using a hierarchy of idealized models. Global
563 darkening—a surrogate for the shortwave scattering effect of volcanic aerosol—leads to a weak-
564 ened stratospheric vortex and equatorward jet shift, broadly the opposite circulation response ex-
565 pected from global warming. In contrast, warming of the tropical lower stratosphere resulting
566 from aerosol absorption of long-wave radiation strengthens the vortex and shifts the jets poleward
567 in both winter hemispheres and the SH summer. This response is found to be remarkably generic,
568 robust to large perturbations of both the boundary conditions and atmospheric physics. Given that
569 stratospheric warming alone appears both qualitatively and quantitatively sufficient to explain the
570 expected circulation response (Robock and Mao 1995; Fischer et al. 2007), we argue that it is the
571 primary driver.

572 Analysis of our model hierarchy indicates that the mechanism involves eddies at a fundamental
573 level in both the stratosphere and troposphere. A naïve argument that the stratospheric warming
574 increases the equator-to-pole temperature gradient (and so strengthening the polar vortex) cannot
575 qualitatively predict the response, and is unhelpful in explaining the surprisingly similar circulation
576 response of the summer hemisphere where there is no vortex mediating stratosphere-troposphere
577 interactions. This supports the conclusions of Bittner et al. (2016), who found that eddies play
578 a critical role in the response of the stratosphere to volcanic eruptions, and the growing body of
579 literature that shows tropospheric eddies are key to mediating the response of the jet stream to the
580 stratosphere (see Kidston et al. 2015, and references therein).

581 A focus on the influence of stratospheric warming on the polar vortices tends to over-emphasize
582 the response in the mid-to-upper stratosphere, which is stronger in the winter hemisphere and

583 more strongly driven by planetary wave forcing (Figure 10). In contrast, the more subtle increase
584 in winds in the lower stratosphere is much more symmetric and independent of season, and thus
585 appears to be more critical in coupling the response to the surface, without requiring strong plan-
586 etary wave generation.

587 The information provided by the equilibrium and switch-on experiments support two pathways
588 for the stratosphere to influence the tropospheric jet streams. The dominant route appears to be
589 through the extratropics, where the stratospheric response leads the troposphere. This pathway is
590 similar to the response to sudden stratospheric warmings and ozone loss. A potential secondary
591 pathway relates to the tropical circulation, where stratospheric warming can disrupt the QBO and
592 thereby influence the troposphere directly through residual circulation in the subtropics Garfinkel
593 et al. (2012). This secondary pathway, however, is substantially weaker, and may not play a
594 meaningful role in the observed response as the residence time of stratospheric aerosols is of the
595 same order as the QBO.

596 Our models suggest that the tropospheric response to stratospheric warming correlates highly
597 with natural variability. Differences of these modes in response to changes in the boundary condi-
598 tions and model physics can thus be used to explain the qualitative differences in the tropospheric
599 response with model configuration, and to a lesser extent, the quantitative differences. The over-
600 lap with natural variability, however leads to a sampling problem, as the surface response is small
601 relative to natural variability, particularly in the NH during winter, where a posteriori we found the
602 weak signal required 81 samples. It is therefore not surprising that other modeling studies have
603 not universally found a measurable impact (e.g., Ramachandran et al. 2000; Robock et al. 2007;
604 Driscoll et al. 2012; Marshall et al. 2009).

605 While the idealization of our models allows us assess the to identify the key dynamical pathways,
606 and assess the robustness of the response, one must always be cautious in applying the results to the

607 real atmosphere. In particular, our approximation of the shortwave effect as an overall reduction of
608 the solar constant neglects the zonal structure of the response and other impacts in the shortwave.
609 Proposed multi-model intercomparison projects such as VolMIP will provide an opportunity to
610 compare the response to shortwave and longwave effects in a comprehensive modeling context.
611 We believe that our comparatively inexpensive model runs provide further justification for the
612 commitment of substantial modeling and computational resources to investigate the circulation
613 response to volcanic eruptions within the CMIP6.

614 *Acknowledgments.* KD and EPG acknowledge support of the National Science Foundation to
615 New York University through grant AGS-1546585. EPG also acknowledges support of Euro-
616 pean Research Commission through project 677756, FORECASToneMONTH for the develop-
617 ment of MiMA. MT acknowledges support from the Deutsche Forschungsgemeinschaft (DFG)
618 in the framework of the priority program “Antarctic Research with Comparative Investigations in
619 Glaciated Areas of the Arctic” through grant TO 967/1-1.

620 **References**

- 621 Alexander, M. J., and T. J. Dunkerton, 1999: A Spectral Parameterization of Mean-Flow
622 Forcing due to Breaking Gravity Waves. *J. Atmos. Sci.*, **56** (24), 4167–4182, doi:10.1175/
623 1520-0469(1999)056<4167:ASPOMF>2.0.CO;2.
- 624 Baldwin, M. P., and T. J. Dunkerton, 2001: Stratospheric Harbingers of Anomalous Weather
625 Regimes. *Science (80-.)*, **294** (5542), 581–584, doi:10.1126/science.1063315.
- 626 Barnes, E. A., S. Solomon, and L. M. Polvani, 2016: Robust wind and precipitation responses to
627 the Mount Pinatubo eruption, as simulated in the CMIP5 models. *J. Clim.*, **29** (13), 4763–4778,
628 doi:10.1175/JCLI-D-15-0658.1.

- 629 Bittner, M., C. Timmreck, H. Schmidt, M. Toohey, and K. Krüger, 2016: The impact of wave-mean
630 flow interaction on the Northern Hemisphere polar vortex after tropical volcanic eruptions. *J.*
631 *Geophys. Res. Atmos.*, **121** (10), 5281–5297, doi:10.1002/2015JD024603.
- 632 Driscoll, S., A. Bozzo, L. J. Gray, A. Robock, and G. Stenchikov, 2012: Coupled Model Inter-
633 comparison Project 5 (CMIP5) simulations of climate following volcanic eruptions. *J. Geophys.*
634 *Res. Atmos.*, **117** (17), doi:10.1029/2012JD017607.
- 635 Fischer, E. M., J. Luterbacher, E. Zorita, S. F. B. Tett, C. Casty, and H. Wanner, 2007: European
636 climate response to tropical volcanic eruptions over the last half millennium. *Geophys. Res.*
637 *Lett.*, **34** (5), doi:10.1029/2006GL027992.
- 638 Franklin, B., 1784: Meteorological imaginations and conjectures. *Manchester Lit. Philos. Soc.*
639 *Mem. Proc.*, Vol. 2.
- 640 Frierson, D. M. W., I. M. Held, and P. Zurita-Gotor, 2006: A Gray-Radiation Aquaplanet Moist
641 GCM. Part I: Static Stability and Eddy Scale. *J. Atmos. Sci.*, **63** (10), 2548–2566, doi:10.1175/
642 JAS3753.1.
- 643 Garfinkel, C. I., T. A. Shaw, D. L. Hartmann, and D. W. Waugh, 2012: Does the Holton–Tan
644 Mechanism Explain How the Quasi-Biennial Oscillation Modulates the Arctic Polar Vortex? *J.*
645 *Atmos. Sci.*, **69** (5), 1713–1733, doi:10.1175/JAS-D-11-0209.1.
- 646 Garfinkel, C. I., D. W. Waugh, and E. P. Gerber, 2013: The effect of tropospheric jet latitude on
647 coupling between the stratospheric polar vortex and the troposphere. *J. Clim.*, **26** (6), 2077–
648 2095, doi:10.1175/JCLI-D-12-00301.1.

649 Gerber, E. P., and L. M. Polvani, 2009: Stratosphere-Troposphere Coupling in a Relatively Simple
650 AGCM: The Importance of Stratospheric Variability. *J. Clim.*, **22** (8), 1920–1933, doi:10.1175/
651 2008JCLI2548.1.

652 Graf, H. F., 1992: Arctic radiation deficit and climate variability. *Clim. Dyn.*, **7** (April 1982),
653 19–28.

654 Graf, H.-F., I. Kirchner, A. Robock, and I. Schult, 1993: Pinatubo eruption winter climate effects:
655 models versus observations. *Clim. Dyn.*, **9**, 81–93.

656 Held, I. M., and A. Y. Hou, 1980: Nonlinear Axially Symmetric Circulations in a Nearly Inviscid
657 Atmosphere. 515–533 pp., doi:10.1175/1520-0469(1980)037<0515:NASCIA>2.0.CO;2.

658 Held, I. M., and M. J. Suarez, 1994: A Proposal for the Intercomparison of the Dynamical Cores
659 of Atmospheric General Circulation Models. 1825–1830 pp., doi:10.1175/1520-0477(1994)
660 075<1825:APFTIO>2.0.CO;2.

661 Holton, J. R., P. H. Haynes, M. E. McIntyre, A. R. Douglass, and B. Rood, 1995: Stratosphere-
662 Troposphere Exchange. *Rev. Geophys.*, **33** (4), 403–439.

663 Holton, J. R., and H.-C. Tan, 1980: The Influence of the Equatorial Quasi-Biennial Oscillation
664 on the Global Circulation at 50 mb. 2200–2208 pp., doi:10.1175/1520-0469(1980)037<2200:
665 TIOTEQ>2.0.CO;2.

666 Iacono, M. J., E. J. Mlawer, S. A. Clough, and J.-J. Morcrette, 2000: Impact of an improved
667 longwave radiation model, RRTM, on the energy budget and thermodynamic properties of the
668 NCAR community climate model, CCM3. *J. Geophys. Res.*, **105** (D11), 14 873, doi:10.1029/
669 2000JD900091.

670 Jucker, M., S. Fueglistaler, and G. K. Vallis, 2014: Stratospheric sudden warmings in an idealized
671 GCM. *J. Geophys. Res.*, **119** (19), 11,054–11,064, doi:10.1002/2014JD022170.

672 Jucker, M., and E. P. Gerber, 2017: Untangling the annual cycle of the tropical tropopause layer
673 with an idealized moist model. *J. Clim.*, **30** (18), 7339–7358, doi:10.1175/JCLI-D-17-0127.1.

674 Karpechko, A. Y., N. P. Gillett, M. Dall’Amico, and L. J. Gray, 2010: Southern Hemisphere
675 atmospheric circulation response to the El Chichon and Pinatubo eruptions in coupled climate
676 models. *Q. J. R. Meteorol. Soc.*, **136** (652), 1813–1822, doi:10.1002/qj.683.

677 Kidston, J., A. A. Scaife, S. C. Hardiman, D. M. Mitchell, N. Butchart, M. P. Baldwin, and
678 L. J. Gray, 2015: Stratospheric influence on tropospheric jet streams, storm tracks and surface
679 weather. *Nat. Geosci.*, **8** (6), 433–440, doi:10.1038/NGEO2424.

680 Kushner, and Polvani, 2004: Stratospheric-tropospheric coupling in a relatively simple AGCM:
681 The role of eddies. *J. Clim.*, **17**, 629–639, doi:10.1175/JCLI4007.1.

682 Kushner, P. J., I. M. Held, and T. L. Delworth, 2001: Southern Hemisphere Atmospheric Circu-
683 lation Response to Global Warming. *J. Clim.*, **14**, 2238–2249, doi:10.1175/1520-0442(2001)
684 014(0001:SHACRT)2.0.CO;2.

685 Lehner, F., A. P. Schurer, G. C. Hegerl, C. Deser, and T. L. Frolicher, 2016: The importance of
686 ENSO phase during volcanic eruptions for detection and attribution. *Geophys. Res. Lett.*, **43** (6),
687 2851–2858, doi:10.1002/2016GL067935.

688 Marshall, A. G., A. A. Scaife, and S. Ineson, 2009: Enhanced seasonal prediction of Eu-
689 ropean winter warming following volcanic eruptions. *J. Clim.*, **22** (23), 6168–6180, doi:
690 10.1175/2009JCLI3145.1.

691 McGraw, M. C., E. A. Barnes, and C. Deser, 2016: Reconciling the observed and modeled South-
692 ern Hemisphere circulation response to volcanic eruptions. *Geophys. Res. Lett.*, **43** (13), 7259–
693 7266, doi:10.1002/2016GL069835.

694 Minnis, P., E. F. Harrison, L. L. Stowe, G. G. Gibson, F. M. Denn, D. R. Doelling, and W. L.
695 Smith, 1993: Radiative climate forcing by the mount Pinatubo eruption. *Science*, **259** (5100),
696 1411–5, doi:10.1126/science.259.5100.1411.

697 Mlawer, E. J., S. J. Taubman, P. D. Brown, M. J. Iacono, and S. A. Clough, 1997: Radiative transfer
698 for inhomogeneous atmospheres: RRTM, a validated correlated-k model for the longwave. *J.*
699 *Geophys. Res. Atmos.*, **102** (D14), 16 663–16 682, doi:10.1029/97JD00237.

700 Niemeier, U., and H. Schmidt, 2017: Changing transport processes in the stratosphere by ra-
701 diative heating of sulfate aerosols. *Atmos. Chem. Phys.*, **17** (24), 14 871–14 886, doi:10.5194/
702 acp-17-14871-2017.

703 Perlwitz, J., and H. F. Graf, 1995: The statistical connection between tropospheric and strato-
704 spheric circulation of the Northern Hemisphere in winter. 2281–2295 pp., doi:10.1175/
705 1520-0442(1995)008<2281:TSCBTA>2.0.CO;2.

706 Polvani, L. M., and P. J. Kushner, 2002: Tropospheric response to stratospheric perturbations in
707 a relatively simple general circulation model. *Geophys. Res. Lett.*, **29** (7), 1114, doi:10.1029/
708 2001GL014284.

709 Polvani, L. M., D. W. Waugh, G. J. P. Correa, and S.-W. Son, 2011: Stratospheric Ozone Deple-
710 tion: The Main Driver of Twentieth-Century Atmospheric Circulation Changes in the Southern
711 Hemisphere. *J. Clim.*, **24** (3), 795–812, doi:10.1175/2010JCLI3772.1.

712 Ramachandran, S., V. Ramaswamy, G. L. Stenchikov, and A. Robock, 2000: Radiative impact
713 of the Mount Pinatubo volcanic eruption: Lower stratospheric response. *J. Geophys. Res.*, **105**,
714 24 409, doi:10.1029/2000JD900355.

715 Revell, L. E., A. Stenke, B. Luo, S. Kremser, E. Rozanov, T. Sukhodolov, and T. Peter, 2017:
716 Impacts of Mt Pinatubo volcanic aerosol on the tropical stratosphere in chemistry-climate model
717 simulations using CCM1 and CMIP6 stratospheric aerosol data. *Atmos. Chem. Phys.*, **17 (21)**,
718 13 139–13 150, doi:10.5194/acp-17-13139-2017.

719 Ring, M. J., and R. A. Plumb, 2007: Forced Annular Mode Patterns in a Simple Atmospheric
720 General Circulation Model. *J. Atmos. Sci.*, **64 (10)**, 3611–3626, doi:10.1175/JAS4031.1.

721 Robock, A., 2000: Volcanic Eruptions and Climate. *Rev. Geophys.*, **38 (2)**, 191–219.

722 Robock, A., T. Adams, M. Moore, L. Oman, and G. Stenchikov, 2007: Southern Hemisphere at-
723 mospheric circulation effects of the 1991 Mount Pinatubo eruption. *Geophys. Res. Lett.*, **34 (23)**,
724 1–6, doi:10.1029/2007GL031403.

725 Robock, A., and J. Mao, 1995: The volcanic signal in surface temperature observations. *J. Clim.*,
726 **8**, 1086–1103, doi:10.1175/1520-0442(1995)008<1086:TVSIST>2.0.CO;2.

727 Roscoe, H. K., and J. D. Haigh, 2007: Influences of ozone depletion, the solar cycle and the
728 QBO on the Southern Annular Mode. *Q. J. R. Meteorol. Soc.*, **133 (October)**, 937–948, doi:
729 10.1002/qj, arXiv:0801.1618v2.

730 Son, S.-W., and Coauthors, 2010: Impact of stratospheric ozone on Southern Hemisphere cir-
731 culation change: A multimodel assessment. *J. Geophys. Res.*, **115**, D00M07, doi:10.1029/
732 2010JD014271.

- 733 Stenchikov, G., A. Robock, V. Ramaswamy, M. D. Schwarzkopf, K. Hamilton, and S. Ra-
734 machandran, 2002: Arctic Oscillation response to the 1991 Mount Pinatubo eruption: Ef-
735 fects of volcanic aerosols and ozone depletion. *J. Geophys. Res. Atmos.*, **107** (24), 1–16, doi:
736 10.1029/2002JD002090.
- 737 Thompson, D. W. J., and J. M. Wallace, 2000: Annular Mode in the Extratropical Circulation. Part
738 I : Month-to-Month Variability. *J. Clim.*, **13** (1999), 1000–1016.
- 739 Thompson, D. W. J., J. M. Wallace, P. D. Jones, and J. J. Kennedy, 2009: Identifying signatures of
740 natural climate variability in time series of global-mean surface temperature: Methodology and
741 insights. *J. Clim.*, **22** (22), 6120–6141, doi:10.1175/2009JCLI3089.1.
- 742 Toohey, M., K. Krüger, M. Bittner, C. Timmreck, and H. Schmidt, 2014: The impact of
743 volcanic aerosol on the Northern Hemisphere stratospheric polar vortex: Mechanisms and
744 sensitivity to forcing structure. *Atmos. Chem. Phys.*, **14** (23), 13 063–13 079, doi:10.5194/
745 acp-14-13063-2014.
- 746 Wittman, M. A. H., L. M. Polvani, R. K. Scott, and A. J. Charlton, 2004: Stratospheric influence
747 on baroclinic lifecycles and its connection to the Arctic Oscillation. *Geophys. Res. Lett.*, **31** (16),
748 1–5, doi:10.1029/2004GL020503.
- 749 Yin, J. H., 2005: A consistent poleward shift of the storm tracks in simulations of 21st century
750 climate. *Geophys. Res. Lett.*, **32**, 1–4, doi:10.1029/2005GL023684.
- 751 Zanchettin, D., and Coauthors, 2016: The Model Intercomparison Project on the climatic response
752 to Volcanic forcing (VolMIP): Experimental design and forcing input data for CMIP6. *Geosci.*
753 *Model Dev.*, **9** (8), 2701–2719, doi:10.5194/gmd-9-2701-2016.

754 **LIST OF TABLES**

755 **Table 1.** Parameter values for the temperature tendency used as warming forcing. 36

756 **Table 2.** Parameter values for temperature tendencies directly applied as warming forc-
757 ing. 37

TABLE 1. Parameter values for the temperature tendency used as warming forcing.

i	a_i (K day ⁻¹)	$\tilde{\phi}_i$ (deg)	\tilde{z}_i (km)	σ_i (deg)	ζ_i (km)
1	0.5	0	24.5	26	4
2	0.08	-36	21	17	3.6
3	0.08	36	21	17	3.6

TABLE 2. Parameter values for temperature tendencies directly applied as warming forcing.

Model	Topography	Season	Hemisphere	Variance ₃₅	ρ_{35}	A_{35}	Variance ₈₅₀	ρ_{850}	A_{850}
MiMA	realistic	DJF	SH	0.66	0.50	0.89	0.53	0.99	0.66
MiMA	realistic	DJF	NH	0.70	0.98	0.47	0.51	0.99	0.23
MiMA	realistic	JJA	SH	0.62	0.54	1.4	0.47	0.98	1.2
MiMA	realistic	JJA	NH	0.43	0.52	1.2	0.37	0.66	0.13
MiMA	flat	DJF	SH	0.81	0.92	1.3	0.69	0.99	0.83
MiMA	flat	DJF	NH	0.56	0.77	1.7	0.61	0.99	0.61
Dynamical core	flat	DJF	SH	0.53	0.97	2.0	0.81	0.96	0.42
Dynamical core	flat	DJF	NH	0.73	0.96	1.2	0.72	0.99	0.26

758 **LIST OF FIGURES**

759 **Fig. 1.** Time-averaged 300 hPa transient eddy kinetic energy per unit mass in MiMA. Contours
760 indicate the coastline on our model grid. 39

761 **Fig. 2.** Equilibrium zonally-averaged temperature and zonal wind responses to surface darkening
762 and stratospheric warming in MiMA. Shading indicates significance at the 95 % confidence
763 level, controlling for false discovery rate. Climatological winds are shown in isotachs of
764 10 m s^{-1} , with easterly isotachs dashed; climatological temperatures are shown in isotherms
765 of 20 K. 40

766 **Fig. 3.** Equilibrium zonally-averaged temperature and zonal wind responses to stratospheric warm-
767 ing in the simplified models. Shading indicates significance at the 95 % confidence level,
768 controlling for false discovery rate. Climatological winds are shown in isotachs of 10 m s^{-1} ,
769 with easterly isotachs dashed; climatological temperatures are shown in isotherms of 20 K. . . . 41

770 **Fig. 4.** Equilibrium streamfunction responses to warming in the axisymmetric and three-
771 dimensional dynamical core. Climatological streamlines are selectively shown in logarith-
772 mic spacing, with negative streamlines dashed. 42

773 **Fig. 5.** Equilibrium DJF zonally-averaged zonal wind responses to unit, doubled, and halved warm-
774 ing in MiMA. Dashed lines indicate $2\times$ and $1/2\times$ multiples of the unit forcing response.
775 43

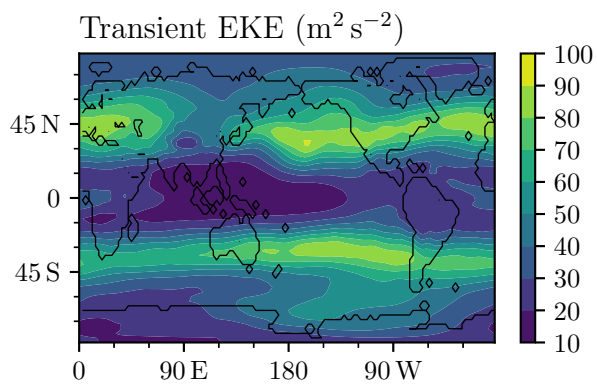
776 **Fig. 6.** Temporal evolution in the stratosphere and troposphere of the zonally-averaged zonal wind
777 responses to warming, following a January 1 abrupt initiation of heating rate anomalies.
778 Note pairs (a,b) and (c,d) each share a color scale. 44

779 **Fig. 7.** Projections of the zonally-averaged zonal wind ensemble response to warming in the three-
780 dimensional dynamical core onto the equilibrium response, averaged over the specified re-
781 gions. Projections are smoothed using a 30-day low-pass Butterworth filter and corrected
782 for group delay; note that low-frequency noise persists. 45

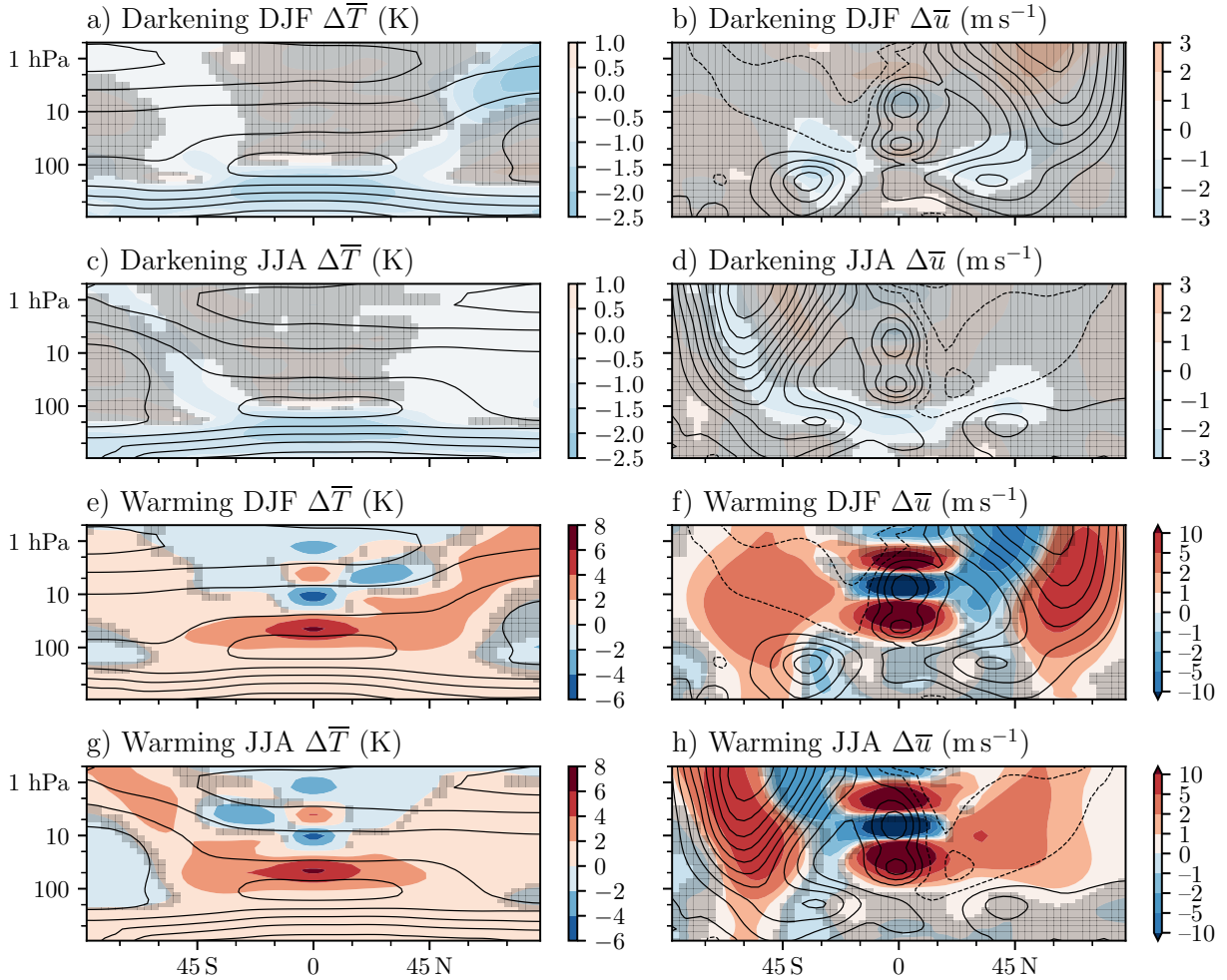
783 **Fig. 8.** Comparison of zonally-averaged zonal wind responses to warming in the three-dimensional
784 dynamical core for equilibrium and ensemble experiments. 46

785 **Fig. 9.** Monthly evolution of the zonally-averaged zonal wind responses to warming in MiMA with
786 a flat lower boundary, following a January 1 abrupt initiation of heating rate anomalies.
787 Climatological winds are shown in isotachs of 10 m s^{-1} , with easterly isotachs dashed. . . . 47

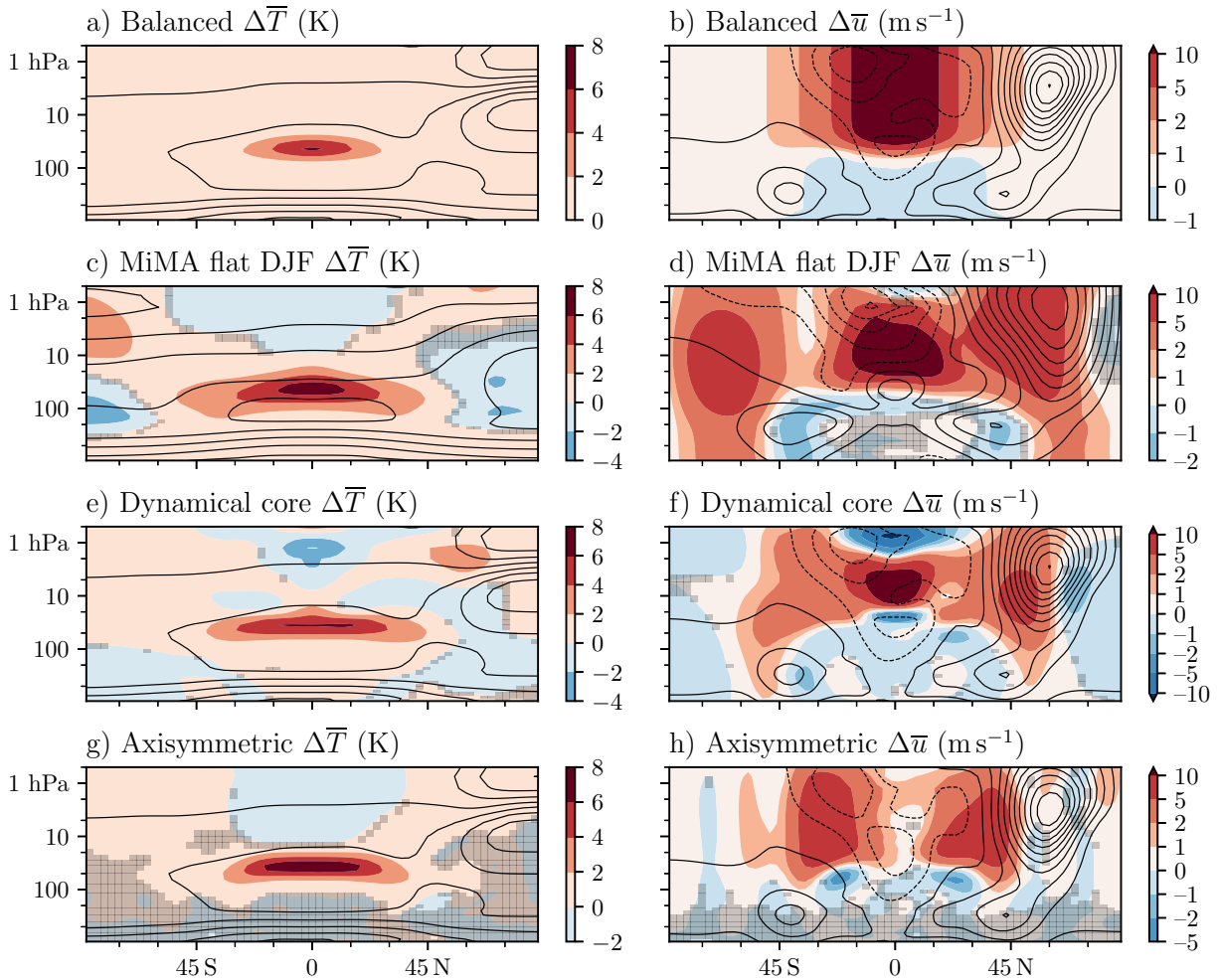
788 **Fig. 10.** Extratropical zonally-averaged zonal wind responses to warming (shaded) and correspond-
789 ing annular modes (contoured in isotachs of 1 m s^{-1} per unit variance, with easterly isotachs
790 dashed) for NH DJF in MiMA (a) with and (b) without topography. 48



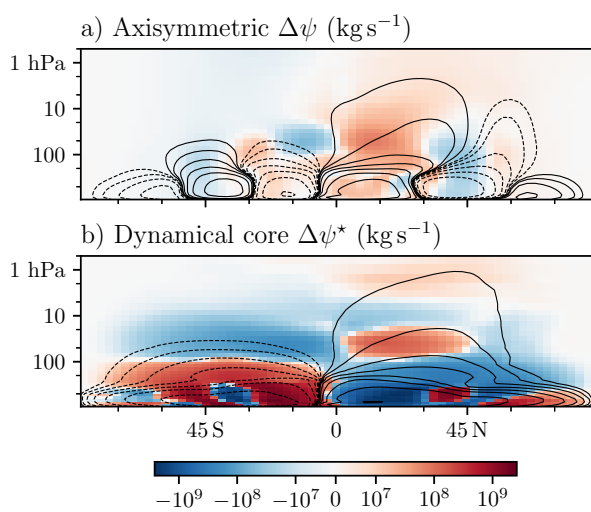
791 FIG. 1. Time-averaged 300 hPa transient eddy kinetic energy per unit mass in MiMA. Contours indicate the
792 coastline on our model grid.



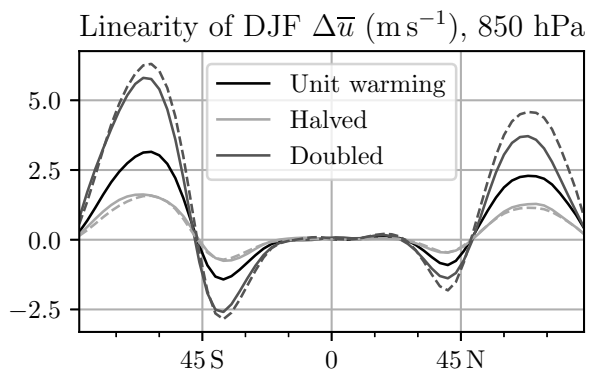
793 FIG. 2. Equilibrium zonally-averaged temperature and zonal wind responses to surface darkening and strato-
 794 spheric warming in MiMA. Shading indicates significance at the 95 % confidence level, controlling for false
 795 discovery rate. Climatological winds are shown in isotachs of 10 m s^{-1} , with easterly isotachs dashed; climato-
 796 logical temperatures are shown in isotherms of 20 K.



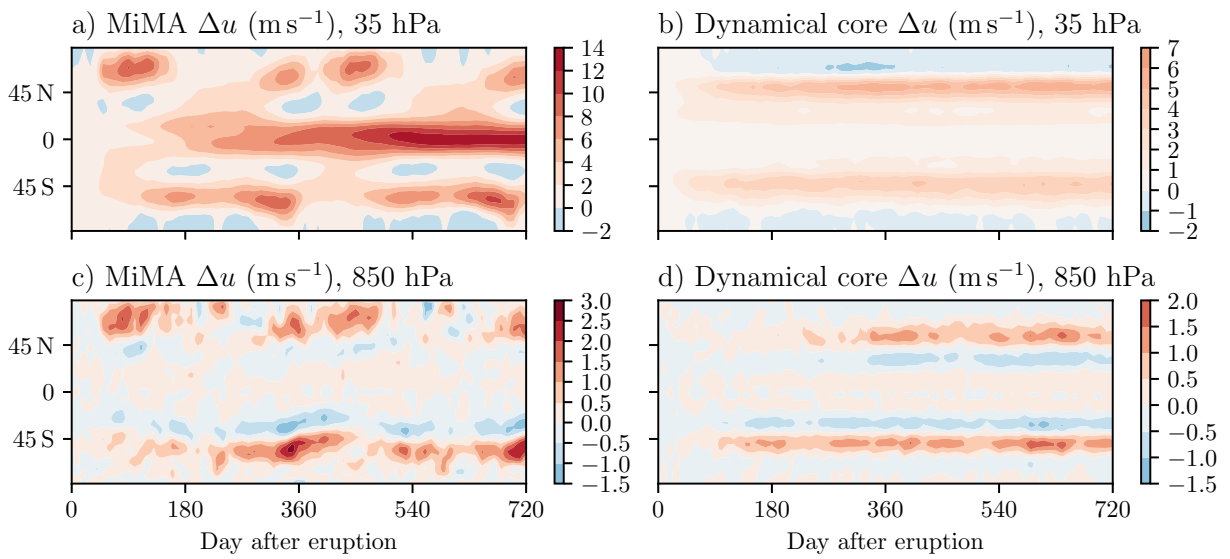
797 FIG. 3. Equilibrium zonally-averaged temperature and zonal wind responses to stratospheric warming in the
 798 simplified models. Shading indicates significance at the 95 % confidence level, controlling for false discovery
 799 rate. Climatological winds are shown in isotachs of 10 m s^{-1} , with easterly isotachs dashed; climatological
 800 temperatures are shown in isotherms of 20 K.



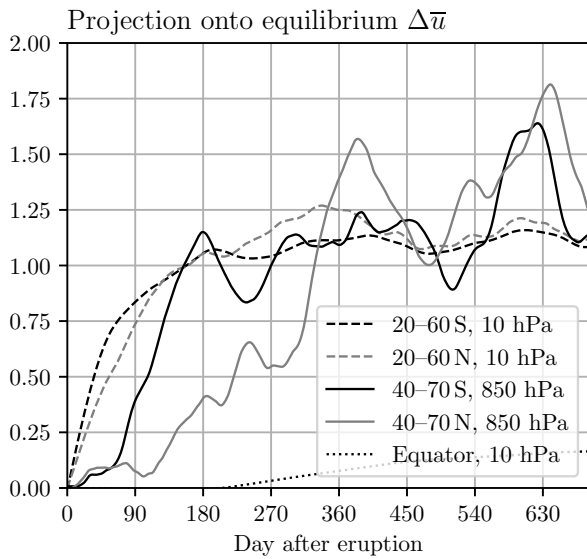
801 FIG. 4. Equilibrium streamfunction responses to warming in the axisymmetric and three-dimensional dynamical core. Climatological streamlines are selectively shown in logarithmic spacing, with negative streamlines
 802 dashed.
 803



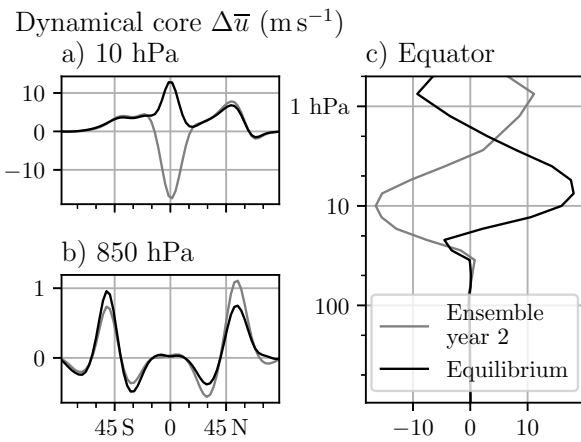
804 FIG. 5. Equilibrium DJF zonally-averaged zonal wind responses to unit, doubled, and halved warming in
 805 MiMA. Dashed lines indicate $2\times$ and $1/2\times$ multiples of the unit forcing response.



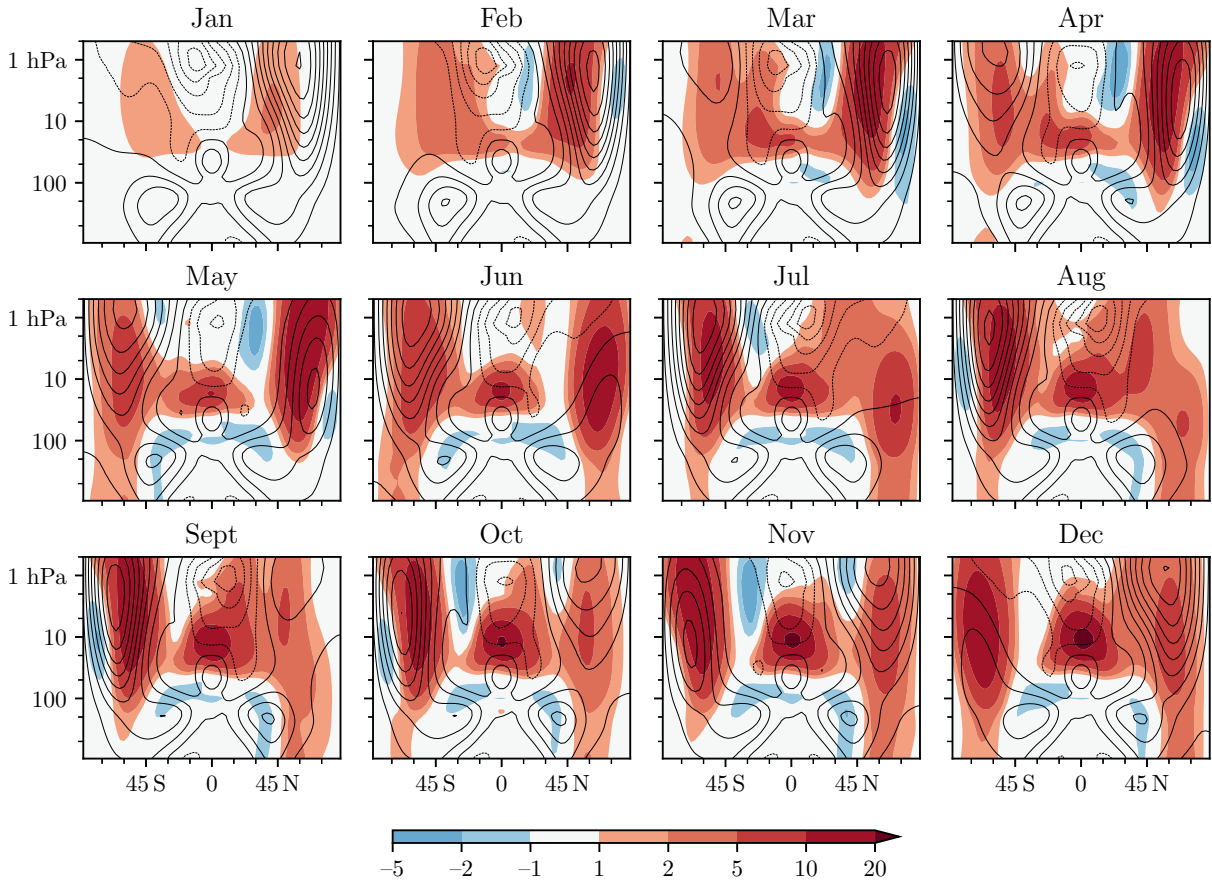
806 FIG. 6. Temporal evolution in the stratosphere and troposphere of the zonally-averaged zonal wind responses
 807 to warming, following a January 1 abrupt initiation of heating rate anomalies. Note pairs (a,b) and (c,d) each
 808 share a color scale.



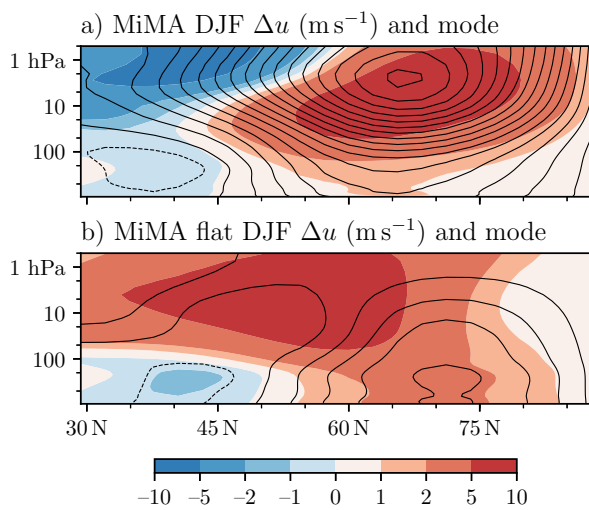
809 FIG. 7. Projections of the zonally-averaged zonal wind ensemble response to warming in the three-
 810 dimensional dynamical core onto the equilibrium response, averaged over the specified regions. Projections
 811 are smoothed using a 30-day low-pass Butterworth filter and corrected for group delay; note that low-frequency
 812 noise persists.



813 FIG. 8. Comparison of zonally-averaged zonal wind responses to warming in the three-dimensional dynamical
 814 core for equilibrium and ensemble experiments.



815 FIG. 9. Monthly evolution of the zonally-averaged zonal wind responses to warming in MiMA with a flat
 816 lower boundary, following a January 1 abrupt initiation of heating rate anomalies. Climatological winds are
 817 shown in isotachs of 10 m s^{-1} , with easterly isotachs dashed.



818 FIG. 10. Extratropical zonally-averaged zonal wind responses to warming (shaded) and corresponding annular
 819 modes (contoured in isotachs of 1 m s^{-1} per unit variance, with easterly isotachs dashed) for NH DJF in MiMA
 820 (a) with and (b) without topography.